Single-Entity Electrocatalysis at Electrode Ensembles Prepared by Template Synthesis

View the article online for updates and enhancements.

Single-Entity Electrocatalysis at Electrode Ensembles Prepared by Template Synthesis

Natasha P. Siepser,* Myung-Hoon Choi, Sasha E. Alden,* and Lane A. Baker*,z

Department of Chemistry, Indiana University Bloomington, Indiana 47405, United States of America

Nanoelectrode ensembles (NEEs), prepared by Au template synthesis, are presented as a proof-of-concept sample platform to study individual electrodeposited materials by scanning electrochemical cell microscopy (SECCM). With this platform, the non-conductive membrane support does not contribute to the electrocatalytic activity recorded at each electrode. Use of low-density template membranes results in electrodes that are isolated because initial membrane pores are typically separated by significant (microscale) distances. Electrodeposition of catalytic nanoparticles onto the electrodes of the array and observation of electrocatalytic activity are demonstrated to be suitable for correlative SECCM voltammetric mapping and electron microscopy. Suitability of NEEs for studies of surface Au oxidation, hydrazine oxidation, and hydrogen evolution (hydrogen evolution reaction, HER), and at Pt particles on NEEs (Pt-NEEs) for HER is demonstrated.
© 2021 The Electrochemical Society ("ECS"). Published on behalf of ECS by IOP Publishing Limited. [DOI: 10.1149/1945-7111/ac44b8]

Supplementary material for this article is available online

Template synthesis is a well-known, versatile strategy for preparing nanoscale electrodes and materials.[1–5] Typically in the template synthesis method, nanomaterials are selectively deposited on or in a support material (the template). Templated synthesis has been applied for diverse nanomaterial geometries,[4–13] including formation of nanowires,[7–9] nanoelectrode arrays,[5,10,14] and nanotubes.[11–13] Templated nanoscale materials have been further studied in a range of applications, including ion transport,[1,3] fundamental electroanalytical measurements,[5,12] and nanomaterial synthesis.[4,8,9,15,16] Track-etched polymeric membranes (e.g. poly-carbonate, poly(ethylene terephthalate), etc.) have been one of the most versatile templates for forming electrode arrays, where nanomaterials deposited can create a random array with location of pores in the membrane controlling the position of resultant electrodes.[1,2,17] A significant advantage of template synthesis is the simplicity for electrode array fabrication, as compared to litho-graphic techniques which require costly instrumentation, albeit, at the expense of limited control in pore patterning of the template. Recently, arrays of gold tubes prepared in porous polymeric membranes by template synthesis, were used as a support for particle electrodeposition and subsequent electroactivity character-ization of the particle samples.[17,18]

Single-entity electrochemical (SEE) measurements, and specifi-cally the study of isolated entities (e.g. nanoparticles), affords the opportunity to understand heterogeneity and distributions beyond typical ensemble measurements. Scanning electrochemical cell microscopy (SECCM), a type of scanned droplet probe microscopy where a droplet hanging from the tip of micro- (or nano-) pipette is scanned across a surface, has emerged as a powerful tool for SEE measurements. In particular, the development of voltammetric hopping mode SECCM,[19] wherein the droplet contacts the sample at a series of predefined locations and a voltammogram is collected at each droplet-sample contact site, has added to the electrochemical information which can be gleaned from a sample compared to electrochemical mapping at a fixed potential. Additionally, the coupling of SECCM with other measurements in correlative multi-microscopy approaches[20–22] has allowed better structure/activity correlation. SECCM measurements have been carried out on a variety of substrate materials including conductors, as in metallic surfaces[23–25] or particles on conductive supports,[21,26,27] semiconductors,[28,29] and insulators.[29,30]

Combining electrode arrays with SECCM for SEE measurements is a compelling concept, as controlling interparticle distances has significant advantages in collecting information on isolated entities. To date, single-entity measurements at electrode arrays by droplet probe techniques remain limited.[31,32] Electrode arrays formed from template synthesis hold additional promise, as the patterned tem-plate, made from an insulating polymeric membrane, results in controlled spacing between isolated electrodes. With subsequent electrodeposition onto electrodes of the array, the properties of isolated nanoparticles could be assessed via SECCM, in contrast to typical samples for SEE, where nanomaterials are drop-cast[21,26,33] or electrodeposited directly on to a conductive support,[27,34] conditions that can often result in aggregated particles. Additionally, when polymer membranes are used as templates, contributions from the underlying substrate to catalytic measurements can be obviated.

Herein, we demonstrate templated nanoelectrode ensembles (NEEs) and Pt particles electrodeposited on top of the NEEs as a new platform for SEE measurements by SECCM. NEEs were prepared from track-etched porous polycarbonate membrane tem-plates that were subjected to Au electroless deposition to deposit Au in the pores of the membrane (Scheme 1). Electrocatalytic activity of NEEs for surface Au oxidation and hydrazine oxidation and NEEs and Pt-NEEs for the hydrogen evolution reaction (HER) were investigated at the single Au tubule or Pt particle level with SECCM voltammetric (CV) mapping.

Experimental

Materials.—Stannous tin chloride ($SnCl_2$), potassium hydroxide (KOH), magnesium oxide (MgO), and sodium bicarbonate ($NaHCO_3$) were used as received from Mallinckrodt. Sulfuric acid (H_2SO_4), formaldehyde, sodium sulfite (Na_2SO_3), chloroform, and nitric acid (HNO_3) were used as received from Macron Fine Chemicals. Chloroauric acid hydrate (>99.9%, $HAuCl_4$ xH_2O), potassium sulfite (K_2SO_3), potassium hexachloroplatinate (IV) (K_2PtCl_6, 98%) were used as received from Sigma-Aldrich. Methanol (MeOH) and hydrochloric acid (HCl) were purchased from Millipore. Silver nitrate ($AgNO_3$), sulfamic acid, and per-chloric acid ($HClO_4$) were used as received from Fischer Scientific. Ammonium hydroxide (NH_4OH, EMD), trifluoroacetic acid (J.T. Baker), and hydrazine hydrate ($N_2H_4\cdot H_2O$, 85% in water, EM sciences) were used as received. Deionized water (18.2 MΩ·cm at 25 °C, Millipore Sigma) was used for all experiments. Ion-tracked polycarbonate (PC) membranes (Osmonics, 10^6 tracks cm^{-2}, 12 μm thick) served as the membrane template. Alumina membranes (Whatman Anodisc) with pore diameters of 0.1 μm were used as

1. Etched polycarbonate membrane

Au electroless deposition

↓

2. Au plated membrane

Remove Au surface film from one face

↓

3. Nanoelectrode ensembles (NEEs)

Pt particle electrodeposition

↓

4. Pt particles on a nanoelectrode ensemble (Pt-NEE)

Scheme 1. Preparation of nanoelectrode ensembles (NEEs) and Pt particles on NEEs (Pt-NEEs).

filters. Pt mesh (99.9% purity, 152 wires/inch) and Pt wire (99.99% purity, 0.6 mm diameter) from Goodfellow were used to assemble a counter electrode. A standard Ag/AgCl (3 M KCl) electrode (BASi) was used as a reference electrode for macroscale electrochemistry.

Preparation of gold(I) sulfite.—Potassium gold(I) sulfite was prepared following a procedure described by Dietz et al.[35] In brief, 0.632 g $KAuCl_4 \cdot xH_2O$ and 0.620 g MgO were added to 5 ml of H_2O (pH = 4) in a round-bottom flask. The bright-yellow suspension was heated in an oil bath at 70 °C with stirring for 30 min, after which the light orange magnesium oxide/magnesium aurate solid was collected by vacuum filtration and rinsed with small quantities of water. A potassium sulfite solution was prepared containing 0.875 g K_2SO_3, 0.375 g sulfamic acid, and 0.360 g KOH in 5 ml H_2O (pH 14) in a round-bottom flask. The dried magnesium oxide/magnesium aurate solid was added to the potassium sulfite solution, heated at 70 °C, and stirred for 30 min, during which time the suspension turned from light orange to pale yellow. The suspension was vacuum filtered to isolate the pale-yellow solid from the clear potassium gold(I) sulfite filtrate. To determine the final Au concentration, an aliquot of the

potassium gold(I) sulfite solution was concentrated and digested in aqua regia. Analysis of the digested solution by liquid-phase ICP-MS at IU Department of Earth and Atmospheric Sciences with an Agilent 7700 quadrupole ICP-MS determined a nominal Au concentration (37.5 g l^{-1}) for the potassium gold(I) sulfite solution.

Preparation of nanoelectrode ensembles (NEEs) in polycarbonate membrane templates.—Fabrication of NEEs in porous membrane templates is depicted in Scheme 1 in which polycarbonate (PC) films are first chemically etched to form etched membranes, followed by electroless deposition of Au which coats the membrane surfaces and pores in the membrane. At extended deposition times, a continuous Au film is formed that covers the faces of the membrane. Mechanical abrasion is used to remove the surface Au film from one membrane face to expose an array of Au tubule electrodes, which are connected through a common base electrode, but isolated spatially from each other by the random location of the pores in the original polymer membrane template. Each step in the fabrication process is further detailed below. Ion-tracked PC films (10^6 tracks cm^{-2}) were immersed in strong base (9 M KOH) to etch latent tracks in the film to form a porous membrane. After 4 h at room temperature, membranes were removed from the etching solution and immersed in a neutralizing solution of 1 M formic acid for 1 h. Membranes were then rinsed and stored in distilled water. The etching process yielded membranes with cylindrical pores (ca. 700 nm in diameter). A modified electroless deposition procedure[2,3] that makes use of galvanic displacement was used to plate gold within the membrane pores and on the membrane surfaces. In brief, membranes were initially soaked in methanol for 6 min, followed by immersion of membranes in a solution of 0.026 M $SnCl_2$ and 0.07 M trifluoroacetic acid in 1:1 methanol:water for 45 min. The Sn-sensitized membranes were then washed twice by immersion in methanol for 3 min in one beaker and then transferring the membranes to a second methanol filled beaker for 3 min. Ammoniacal silver nitrate was prepared from an aqueous solution of 0.029 M $AgNO_3$ that was colorimetrically titrated (from clear to brown to clear again) with ammonia hydroxide. Sn-sensitized membranes were immersed in ammoniacal silver nitrate solution for 7.5 min. After Ag deposition, membranes were soaked sequentially in two portions of methanol (3 min each). An aqueous Au plating solution was prepared from 0.127 M Na_2SO_3, 0.625 M formaldehyde, and 4.80×10^{-3} M gold(I) sulfite in water at a temperature of 2 °C. The pH of the Au plating solution was adjusted to pH 10 by dropwise addition of dilute, cold H_2SO_4 (1:40 concentrated H_2SO_4:H_2O). Ag-functionalized PC membranes were placed in a stirred Au plating solution at 2 °C overnight. The temperature of the Au plating solution was controlled via a water bath recirculator. Following overnight plating, analysis by electron microscopy revealed (*vide infra*) membranes with faces covered with a Au film and pores filled with Au tubules. Gold-plated membranes were soaked in water overnight and then immersed in 25% HNO_3 for 4 h to dissolve residual Sn and Ag on the membrane. Membranes were finally washed in water for several hours and then air dried.

To form an electrode array, one side of the gold-plated membrane was attached to double-sided copper tape (3 M) affixed to a glass slide. The gold film on the membrane face not in contact with the copper tape was removed by pressing a piece of tape (Scotch brand 3650) to the Au film and then peeling the tape off the membrane to expose the Au tubule ends within the membrane template.[2,36] The membrane surface was further scrubbed with a cotton swab wetted with ethanol to remove residual Au from the membrane surface. Prior to electrochemical measurements, NEEs on the copper tape/ glass slide were covered by a tape mask (Scotch brand 3650 with a hole punched in the middle) to define the area of Au tubule ensembles and to insulate the copper tape. NEEs were further cleaned electrochemically by mounting the membrane sample in a U-tube cell, where a perchloric acid solution was added to the half-cell facing the NEEs. Three cyclic voltammetric cycles in 0.1 M $HClO_4$ at 100 mV s^{-1} from −0.3 to 1.4 V were collected, with a Pt

mesh counter electrode and a Ag/AgCl (3 M NaCl) reference electrode. All macroscale electrochemical measurements were carried out using a CHI 660 potentiostat (CH instruments). Lastly, samples were thoroughly rinsed with water.

Electrodeposition of Pt particles.—Pt particles were formed on top of the exposed Au tubules by immersing the NEEs to a stirred solution of 2 mM K_2PtCl_6 in 0.1 M H_2SO_4 while applying a potential program[32] suitable to initiate electrodeposition. Specifically, Pt particles were electrodeposited with the following potential program vs Ag/AgCl (3 M NaCl): $E_1 = 0.41$ V for 1 s, $E_2 = -0.34$ V for 0.4 s, followed by a square wave potential at a frequency of 100 Hz for 30 min with $E_3 = 0.61$ V and $E_4 = 0.21$ V.

Characterization of the polycarbonate membrane and Au tubules.—Membranes, NEEs, standing Au tubules, and the liberated Au tubules were sputter coated (Denton Desktop V) with ca. 4 nm of Au/Pd prior to scanning electron microscopy (FEI Quanta 600 or Zeiss Auriga 60).

Probe fabrication.—Dual barrel borosilicate capillaries (BT-150-10, Sutter Instruments) were pulled (program—Heat: 700, Pull: 0, Velocity: 16, Time 35) on a heated filament pipette puller (P-97, Sutter Instruments) to fabricate dual barrel micropipette probes. Micropipette probes possessed a nominal outer tip diameter of 2–3 μm. Micropipettes were back filled with 10 mM $HClO_4$ or 2 mM $N_2H_4 \cdot H_2O$ and 10 mM $HClO_4$ using a MicroFil syringe (World Precision Instruments Inc.). To prepare electrodes for SECCM, the coating on perfluoroalkoxy coated silver wires (PFA, A−M Systems, Sequim, WA) was removed, followed by chloridizing the exposed silver wires. Ag/AgCl wires were back inserted into each barrel of the solution filled pipette to serve as quasi-reference counter electrodes (QRCEs) for SECCM measurements.

SECCM voltammetric mapping.—Local electrocatalytic measurements were carried out with SECCM voltammetric mapping. A detailed explanation of the SECCM instrumentation employed has been described elsewhere.[21] Briefly, a solution filled dual barrel micropipette, containing Ag/AgCl QRCEs in each barrel, and with a hanging droplet at the tip of the pipette serve as the SECCM probe. A constant 10 mV potential bias (V_1) was applied between the two QRCEs to generate an ion conductance current from the migration of ions across the hanging droplet and the pipette was vertically modulated at 1 kHz with an oscillation height of 100 nm (Fig. 1). Changes in the alternating current (AC) component of the ion current were used as feedback to control the movement of the pipette such that the pipette is approached towards the sample until the droplet contacts the sample surface. For CV acquisition, the probe approached the surface until the droplet contacted the substrate, then following a 1 s hold time (to allow for droplet stabilization), a cyclic voltammogram (CV) was collected (scan rate: 0.5 V s^{-1}) by sweeping the potential (V_2) while the faradaic current generated from the potential sweep was measured by the current amplifier connected to the substrate. After CV collection, the pipette was retracted from the substrate (typically 5–6 μm) to break droplet contact with the surface, and the sample was translated laterally in the XY-direction for the next landing site. This process of hopping the pipette across the sample surface to collect CVs at predefined locations was repeated to construct a SECCM CV (or voltammetric) map.

An environmental chamber was designed to fit around the sample and pipette tip to constantly purge the chamber with humidified nitrogen or argon gas (Fig. S1 available online at stacks.iop.org/JES/168/126526/mmedia). The relative humidity and temperature were monitored near the sample and pipette tip using a temperature/humidity sensor (SHT85, Sensirion AG) and the sensor reading was recorded on a computer with custom script. SECCM measurements were initiated after 5 min of purging the chamber with gas.
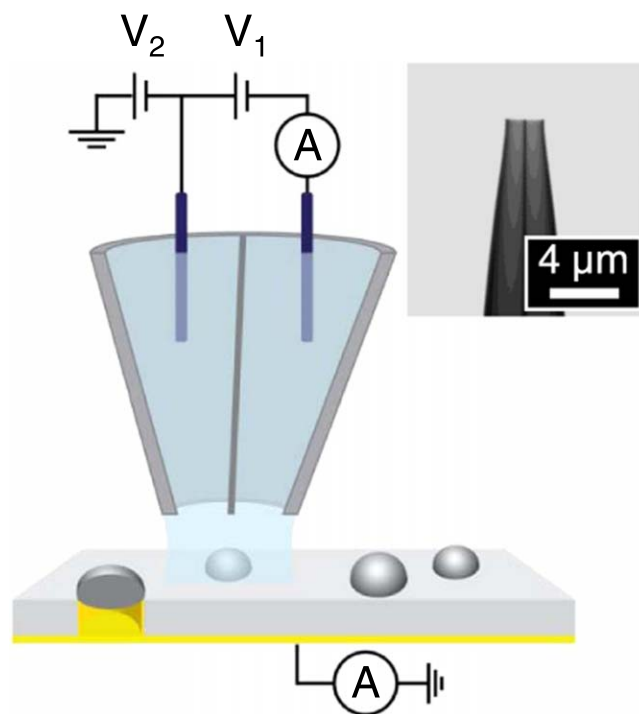

Figure 1. SECCM setup for voltammetric mapping at Pt particles deposited on a nanoelectrode ensemble (Pt-NEE). Inset: Electron micrograph of a dual barrel pipette which serves as the SECCM probe.
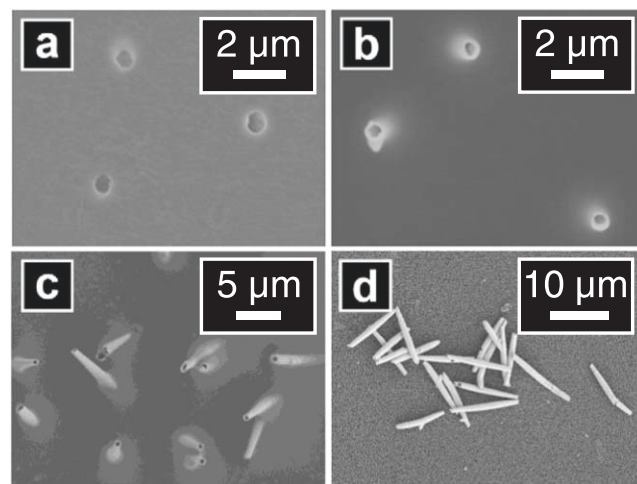

Figure 2. Electron micrographs of an etched polycarbonate (PC) membrane (a) before and (b) after Au electroless deposition. Micrographs of (c) standing cylindrical Au tubules and (d) Au tubules liberated from the membrane template.

All potentials reported for SECCM voltammetric maps were reported vs Ag/AgCl (3 M KCl). Prior to SECCM measurements, Ag/AgCl QRCEs were calibrated to a commercial Ag/AgCl (3 M KCl) electrode. The Ag/AgCl wires were back inserted into a broken pipette that was filled with aqueous 10 mM $HClO_4$. The tip of the broken pipette was immersed in an electrochemical cell containing 10 mM $HClO_4$ and the open-circuit potential was recorded with a potentiostat between each Ag/AgCl wire and a commercial Ag/AgCl (3 M KCl) electrode. The potential recorded was ca. 0.220 V vs Ag/AgCl (3 M KCl).

A TEM grid (1GC75, Pelco) was taped on top of the samples before SECCM voltammetric mapping so that the SECCM probe could be lowered into one of the square holes on the TEM grid

which could be used later to correlate SECCM and SEM measurements. Two optical cameras positioned 90° from each other were used to monitor the pipette tip as the pipette was lowered towards the sample.

Results and Discussion

The membrane template, which served as the platform for fabrication of nanoelectrode ensembles (NEEs), was prepared by chemical etching an ion-tracked polycarbonate (PC) membrane to create pores with diameters of ca. 700 nm (Fig. 2a). Au electroless deposition on the etched PC membrane template resulted in Au plating along the pore walls, to form Au tubules, and a surface film of Au on the two membrane faces. The Au surface film was removed from one membrane face to expose the ends of the Au tubules in the PC membrane template. Since electroless deposition begins on the functionalized membrane surface,[2] nanotubule electrodes of the NEE are templated by the pore structure, resulting in Au tubules with the same outer diameter as the initial pores present in the membrane (700 nm). The thickness of the walls of the tubules was ca. 100 nm determined from an electron micrograph (Fig. 2b). The three-dimensional organization of the arrayed tubules was characterized by affixing one face of the Au plated membrane to Cu tape while the Au surface film on the opposing side of the membrane was removed, and then immersing the NEEs in chloroform to dissolve the PC membrane, which resulted in free standing Au tubules (Fig. 2c). To further characterize tubule morphology, Au tubules were liberated from the PC membrane template completely by removing the Au surface film from both faces with tape and then immersing the membrane in chloroform to dissolve the PC membrane. The suspension of Au tubules in chloroform was then drop-cast onto an alumina membrane, which was examined by electron microscopy, to reveal long cylindrically shaped tubules (Fig. 2d) with lengths comparable to what is expected (12 micron) for the thickness of membrane used. The shape and length of the tubules demonstrates that the rate of electroless plating was appropriate to uniformly deposit Au through the entire length of the membrane. Tubules that span the entire length of the PC membrane and are in electrical contact with the Au surface film on the membrane face were essential to provide a platform for particle electrodeposition and SECCM mapping.

To demonstrate NEEs as a sample platform for SECCM CV mapping, surface gold electrooxidation was investigated first. Electrooxidation of Au when the SECCM probe contains 10 mM $HClO_4$ can be observed for individual Au tubules in the SECCM CV map on a NEE at a substrate bias of 1.34 V vs Ag/AgCl (3 M KCl) (Fig. 3a and in Fig. S2). At each pixel in the SECCM CV map, a CV was collected by sweeping the potential from 0.2 V to 1.34 V vs Ag/AgCl (3 M KCl) at a scan rate of 0.5 V s^{-1}. Darker colored pixels in the CV map correspond to droplet landing positions in which current was recorded for surface oxidation of Au tubules, whereas lighter colored pixels are locations where the SECCM droplet contacted the bare PC membrane, which is an insulator, and thus results in low current. The SECCM mapping area was correlated to the mapped area on the sample with electron microscopy (Fig. 3b). Following SECCM CV mapping, a periodic pattern of salt residue, a remnant from contact by the SECCM droplet on the NEE, was visible on the sample surface. The salt residue, or droplet footprints, a common feature in SECCM measurements,[23,24,37,38] on the NEE surface make a comparison of the SECCM current response to the precise location where the droplet contacted the sample possible. The electron micrograph of the 48 μm by 28 μm mapped area (Fig. 3b) shows a total of 8 Au tubules in the mapped area, wherein 4 Au tubules were contacted by the SECCM droplet, and 2 of the 4 Au tubules contacted by the droplet showed enhanced current signal for gold oxidation (denoted by dotted green circles in Figs. 3a, 3b). Under conditions here, half of the Au tubules in the mapped area were not contacted by the SECCM droplet because the regular spacing between droplet landing sites of SECCM naturally misses

the stochastic location of electrodes in the NEE prepared by ion tracking. The relationship between hopping distance and entity spacing will be described further during the discussion for Fig. 5. Two Au tubules contacted by the SECCM droplet did not show current enhancement (denoted by the solid green circles in Figs. 3a, 3b) possibly because of poor electrical contact between the tubule and the underlying conductive Au film on the bottom of the NEE. Voltammetric responses at two Au tubules that exhibited enhanced current response and one representative position on the bare PC membrane (highlighted by the white circles in Figs. 3a, 3b) were separated into two plots for clarity: voltammetric response during the anodic and cathodic sweeps in Figs. 3c and 3d, respectively. Of note, the bare PC membrane (red trace in Figs. 3c, 3d) showed a featureless voltammogram with low current signal. In the anodic sweep, an enhancement in current at Au tubules #1–2 for Au surface oxidation began ~1.0 V vs Ag/AgCl (3 M KCl) and increased in magnitude as the potential was swept more positive for surface oxidation of the Au tubules. In the reverse (cathodic) sweep, an oxidative current was recorded from 1.34 to 1.2 V vs Ag/AgCl (3 M KCl) at Au tubules #1–2. As the potential was swept more negative than ca. 1.2 V, Au tubule #1 exhibited zero current whereas Au tubule #2 showed a cathodic peak centered around 0.8 V vs Ag/AgCl (3 M KCl) for the reduction of Au oxide. The potential region at which Au surface oxidation and the reduction of Au oxide were observed in the CVs collected by SECCM agrees well with macroscale CVs collected on Au electrodes.[39,40] The greater current signal recorded at Au tubule #2 likely stems from a larger surface area of the Au tubule that was wetted by the SECCM droplet compared to droplet contact to Au tubule #1. Electron micrographs showing droplet contact to Au tubules #1 and #2 in Figs. 3e–3f, respectively, support this conclusion because Au tubule #2 (in Fig. 3f) had rougher surface morphology on the portion of the tubule contacted by the SECCM droplet. Furthermore, Figs. 3e–3f also show a ~2 μm diameter droplet footprint, which is comparable to the tip diameter of the SECCM probe, indicating the reproducibility of droplet contact on the NEE. These baseline measurements were repeatable over multiple samples and highlight the opportunity that NEEs combined with SECCM provide for making electrochemical measurements.

Electrooxidation of hydrazine ($N_2H_5^+ \rightarrow N_2 + 5H^+ + 4e^-$), which serves as an additional system to highlight the application of NEEs for SECCM, was also studied. A SECCM CV map and correlative electron micrograph on a NEE is shown in Figs. 4a, 4b (see also Fig. S3) in which locations for three Au tubules and one representative position on bare PC membrane are highlighted by the green and white circles, respectively. In the 45 μm by 35 μm mapped area there are a total of 17 Au tubules in which 3 of the Au tubules were contacted by the SECCM droplet and showed enhanced current signal for hydrazine oxidation. The other 14 Au tubules in the mapped area were not contacted by the SECCM droplet for the same reasons described for Fig. 3. The CV responses for the anodic and cathodic sweeps are separated for clarity in Figs. 4c and 4d, respectively. In the anodic sweep, oxidation current that is greater than the low current response on the bare PC membrane is observed for Au tubules #3–5 when the potential is > 1.0 V vs Ag/AgCl (3 M KCl). In the cathodic sweep, Au tubules #3–5 exhibit a decreasing oxidative current as the potential is swept from 1.3 to 1.0 V vs Ag/AgCl (3 M KCl) followed by an oxidative peak between 1.0 and 0.6 V vs Ag/AgCl (3 M KCl). The variation in current response at Au tubules #3–5 may be attributed to variation in surface area of the Au tubule wetted by the droplet footprint. Although, we would note that Hill and coworkers performed detailed studies of hydrazine oxidation and reduction on individual solution synthesized gold nanorods (Au NRs) with optically targeted electrochemical cell microscopy, a variation of SECCM, and found the electrochemical response displays complex kinetic effects that likely arise due to differences in each individual NR.[33] Further, voltammograms on individual NRs evolved in multiple scans in a manner that was difficult to quantify.[33] As the point of this report is
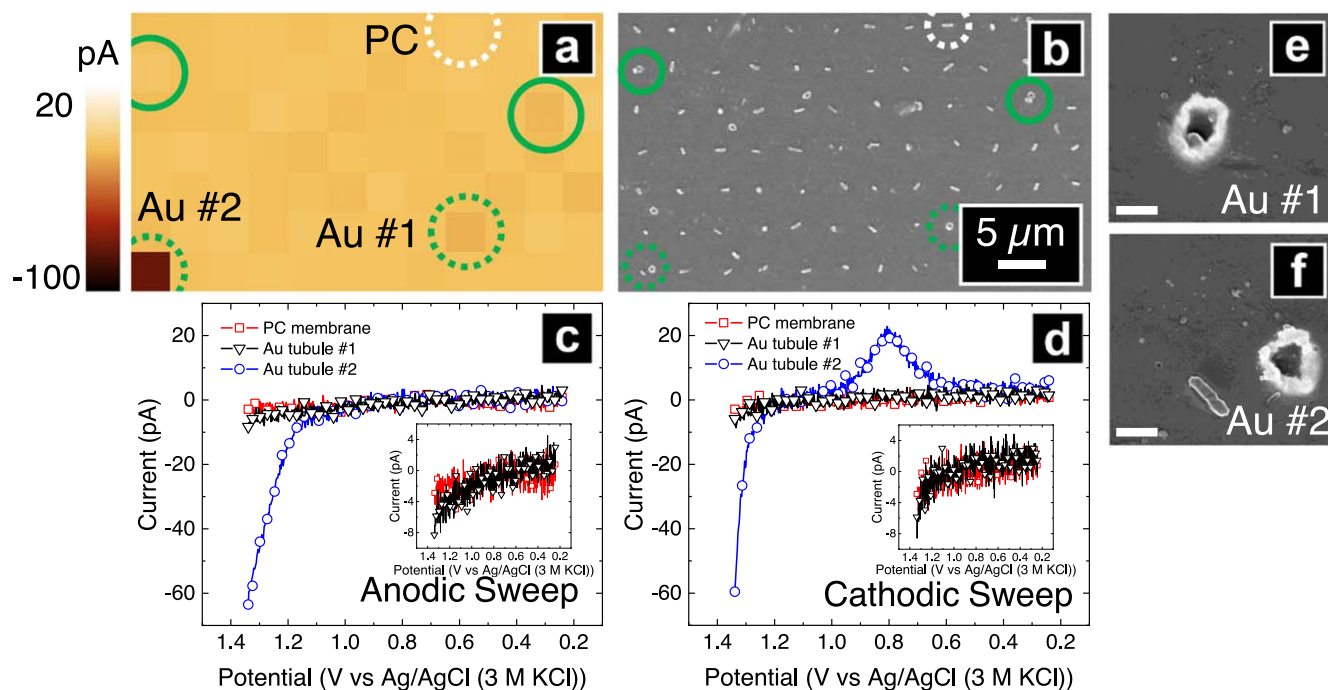
Figure 3. (a) SECCM cyclic voltammetric (CV) map for Au electrooxidation on a nanoelectrode ensemble (NEE) at a substrate bias of 1.34 V vs Ag/AgCl (3 M KCl) and (b) correlative electron micrograph of the same area. The scale bar in Fig. 3b applies to Fig. 3a. (c) Anodic and (d) cathodic voltammetric sweeps at 3 positions: polycarbonate (PC) membrane and Au tubules #1-2. Insets: Zoomed-in voltammetric sweeps at PC membrane and Au tubule #1. (e)–(f) High-resolution electron micrographs of each individual Au tubule (Au tubule #1-2, respectively) exhibiting electrocatalytic current (scale bar = 500 nm). The solution in the pipette was aqueous 10 mM HClO$_4$ and the scan rate was 0.5 V s^{-1}. The spacing between droplet contact spots was 4 μm. The solid green circles denote positions where Au tubules were contacted by the SECCM droplet, but no enhanced current response was recorded.
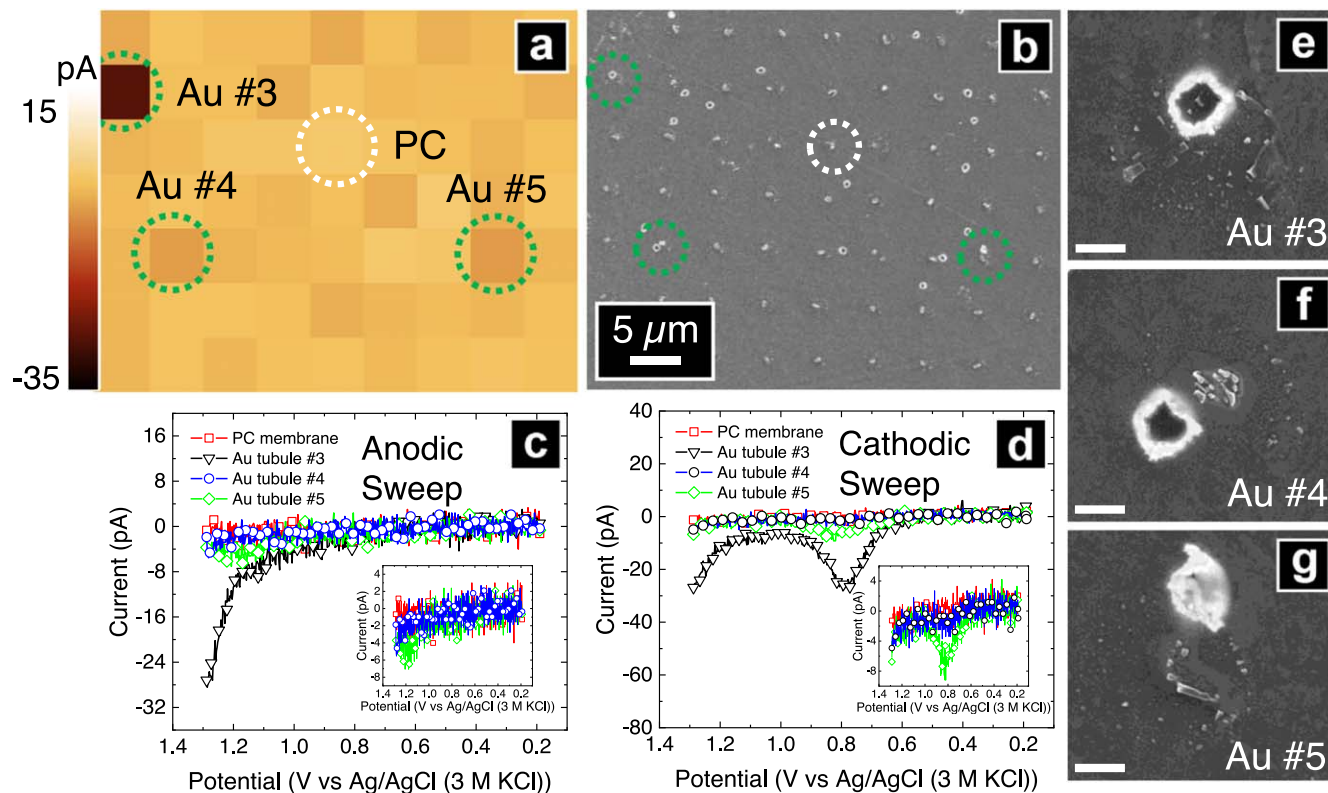

Figure 4. (a) SECCM cyclic voltammetric (CV) map for hydrazine electrooxidation on a nanoelectrode ensemble (NEE) at a substrate bias of 1.3 V vs Ag/AgCl (3 M KCl) and (b) correlative electron micrograph of the same area. The scale bar in Fig. 4b applies to Fig. 4a. (c) Anodic and (d) cathodic voltammetric sweeps at 4 positions: polycarbonate (PC) membrane and Au tubules #3–5. Insets: Zoomed-in voltammetric sweeps at PC membrane and Au tubules #4 and #5. (e)–(g) High-resolution electron micrographs of each individual Au tubule (Au tubule #3–5, respectively) exhibiting electrocatalytic current (scale bar = 500 nm). The solution in the pipette was aqueous 2 mM N$_2$H$_4$·H$_2$O and 10 mM HClO$_4$ and the scan rate was 0.5 V s^{-1}. The spacing between droplet contact spots was 5 μm.

to examine the sample preparation strategy, we did not investigate these effects further. Electron micrographs show the Au tubule morphology and extent of droplet footprint with Au tubules #3–5 in Figs. 4e–4g, respectively. The oxidative current observed at potentials between 1.0 V and 1.3 V vs Ag/AgCl (3 M KCl) in Figs. 4c, 4d are likely from a convolution of gold oxidation and hydrazine electrooxidation because oxidative current was also observed for gold surface oxidation in this potential window (Figs. 3c, 3d). Of note, the anodic peak in Fig. 4d is only visible when the solution in the pipette contains hydrazine, therefore, this anodic peak is attributed to hydrazine oxidation alone. Data recorded here for Au tubules, which shows a peak-shaped response on the cathodic trace, agree well with results described by Hill and coworkers that showed a surface-mediated process for hydrazine oxidation at nanoscale Au.[33] They attributed the oxidative current recorded at single NRs to hydrazine oxidation alone because the expected current from Au/Au$_2$O$_3$ surface reactions at a single Au NR (edge length ~50 nm and width ~20 nm), estimated to be ~10 fA, would be too small to measure with their instrument. In contrast, Au surface oxidation on the NEEs did result in a measurable current by SECCM (Fig. 3) because the Au tubules were larger than the Au NRs studied by the Hill group. Of note, finite element simulations for hydrazine oxidation at a single Au NR suggest that hydrazine oxidation is influenced by Au/Au$_2$O$_3$ surface reactions.[33] Analysis of the NEE by SECCM in the presence and absence of hydrazine demonstrate the convolution of hydrazine electrooxidation and Au surface reactions at individual Au tubules.

A limitation of carrying out SECCM measurements on NEEs prepared from track-etched membranes by template synthesis is the random spatial distribution of electrodes in the ensemble which complicates the utility of SECCM mapping to measure the electrochemical response of multiple electrodes within a single CV map. Strategies, such as increasing the SECCM probe size to increase the droplet diameter contacting the NEE or utilization of a membrane template with a higher density of pores, would increase the likelihood of SECCM droplet contact to electrodes in the NEE, but would also increase the chances of droplet contact to multiple electrodes at a time. Alternatively, more electrodes can be contacted by the SECCM droplet in a mapped area by decreasing the distance between droplet landing sites within a SECCM CV map. In Fig. 5a, SECCM CV mapping on a NEE for hydrazine electrooxidation was carried out with a 2 μm spacing between droplet contact spots. The correlative SEM image of the mapped area (Fig. 5b) revealed that in the 34 μm by 20 μm mapped area there were 8 tubules present in which 6 tubules were contacted and 2 tubules were not contacted by the SECCM droplet. Of the tubules contacted by the droplet, 3 tubules showed enhanced current signal for hydrazine oxidation and 3 tubules showed no current response (denoted by dotted and solid green circles in Figs. 5a, 5b, respectively). The 3 tubules that showed no enhanced current response could be because of poor electrical contact between the Au tubule and the Au film on bottom of the NEE. The 3 Au tubules demonstrating enhanced current response correspond to two pixels in the CV map because the droplet contacted one tubule at one landing site (Au tubule #6) and two tubules at another landing site (Au tubules #7–8) as confirmed by SEM (Figs. 5b and 5e, 5f). The anodic and cathodic sweeps at Au tubules #6–8 and a representative position on the PC membrane (denoted by the white circle in Figs. 5a, 5b) are shown in Figs. 5c, 5d wherein an oxidative current was recorded at the Au tubules and low current response was recorded on the PC membrane. The voltammetric response at Au tubules #7–8 exhibited a current spike ca. 0.95 V in the anodic sweep (Fig. 5c) likely from a sudden increase in the Au surface area wetted by the SECCM droplet during CV collection. Thus, for the random electrode spacing of templated NEEs examined here, decreasing the spacing between droplet landing sites in the SECCM CV map is a method to increase the number of Au tubules contacted by the droplet in the mapped area.

To further demonstrate NEEs as a sample platform for SECCM CV mapping, the hydrogen evolution reaction (HER) was selected as

a model reaction. In Fig. 6a (and Fig. S4a), a SECCM CV map of a NEE at −0.8 V vs Ag/AgCl (3 M KCl) is shown where the lighter colored pixels represent locations where the SECCM droplet contacted a Au tubule exhibiting electrocatalytic current for HER, whereas the dark colored pixels correspond to droplet contact to the bare PC membrane, which exhibits low current response. The SECCM CV map was correlated to the mapped area on the sample using SEM (Figs. 6b and S4b). In the 48 μm by 24 μm mapped area, there were 13 Au tubules wherein 2 of 13 tubules were contacted by the SECCM droplet and exhibited current signal for HER. The other 11 tubules were not contacted by the SECCM droplet. Three positions contacted by the SECCM droplet are highlighted by green and white circles representing droplet contact to Au tubules and bare PC membrane, respectively (Figs. 6a, 6b). Extracted CVs at these three positions are compared in Fig. 6c. In agreement with the previously described SECCM CV maps, the bare PC membrane (red trace in Fig. 6c) showed a featureless voltammogram with low current signal, while the CVs acquired at two Au tubules (Au tubule #9 and #10 in the black and blue traces, respectively) show electrocatalytic current for HER. Hysteresis present in the CVs at Au tubules is attributed to capacitive charging of the tubule. A larger current was recorded at Au tubule #10 because more of the tubule surface area was wetted by the droplet compared to Au tubule #9. The morphology of Au tubules #9–10 and SECCM droplet contact was verified by SEM (Figs. 6d, 6e) in which a ~2 μm diameter droplet footprint, comparable to the tip diameter of the SECCM micropipette probe, encapsulates the Au tubules. Analysis of the NEEs with SECCM for HER underscores the versatility of the NEEs for both reduction reactions (HER) and oxidation reactions as described previously.

NEEs can also serve as a platform for particle electrodeposition, where particles are deposited on top of the open Au tubules, as employed here to create Pt particles on a NEE (Pt-NEE) for single-entity measurements by SECCM. A SECCM CV map at −0.35 V vs Ag/AgCl (3 M KCl) (Fig. 7a) and corresponding electron micrographs (Fig. 7b) of the mapping area at a Pt-NEE demonstrate that enhanced current recorded in the CV map correlate with a SECCM droplet landing site that contacted a Pt particle. In the 56 μm by 24 μm mapped area, there were 11 Au tubules: 9 of the 11 Au tubules had Pt particles deposited on top of the Au tubules and 2 Au tubules did not obviously have Pt particles deposited on them. This suggests that for the 2 Au tubules where Pt deposition did not occur, there is a discontinuity in the Au tubule that prevents electrodeposition, supporting previous observations where no electrocatalytic response was recorded at some Au tubules for Au oxidation, hydrazine oxidation, or HER. This is likely a consequence of the flexible nature of the polymer membranes used as templates which may lead to cracks in electrodeposited tubules during routine handling. The SECCM droplet contacted and measured current signal for HER at one Pt particle deposited on top of a Au tubule in the Pt-NEE mapped area. The other 8 particles in the mapping area were not contacted by the SECCM droplet. The two Au tubules on the Pt-NEE where no Pt particles were deposited was (again) likely from poor electrical contact between these Au tubules and the conductive Au surface film on the bottom membrane face. Two SECCM droplet contact positions, at a Pt particle and the bare PC membrane, are highlighted by the green and white circles, respectively, in Figs. 7a, 7b and the voltammetric response at these positions were analyzed (Fig. 7c). The voltammetric response on the PC membrane (red trace in Fig. 7c) exhibited low current response while the CV at the Pt particle (black trace in Fig. 7c) demonstrated electrocatalytic activity for HER and hysteresis between the forward and reverse traces attributed to capacitive charging of the Pt particle. The double layer capacitance from the SECCM measurement at the Pt particle, in Fig. 7c, was estimated to be ~100 μC cm^{-2} by measuring the capacitance in the cathodic sweep in the CV collected at the Pt particle prior to the onset for HER where the current value is near-constant (i.e. −0.1 V to −0.12 V) and assuming that the Pt particle is spherical. The double layer capacitance was calculated by
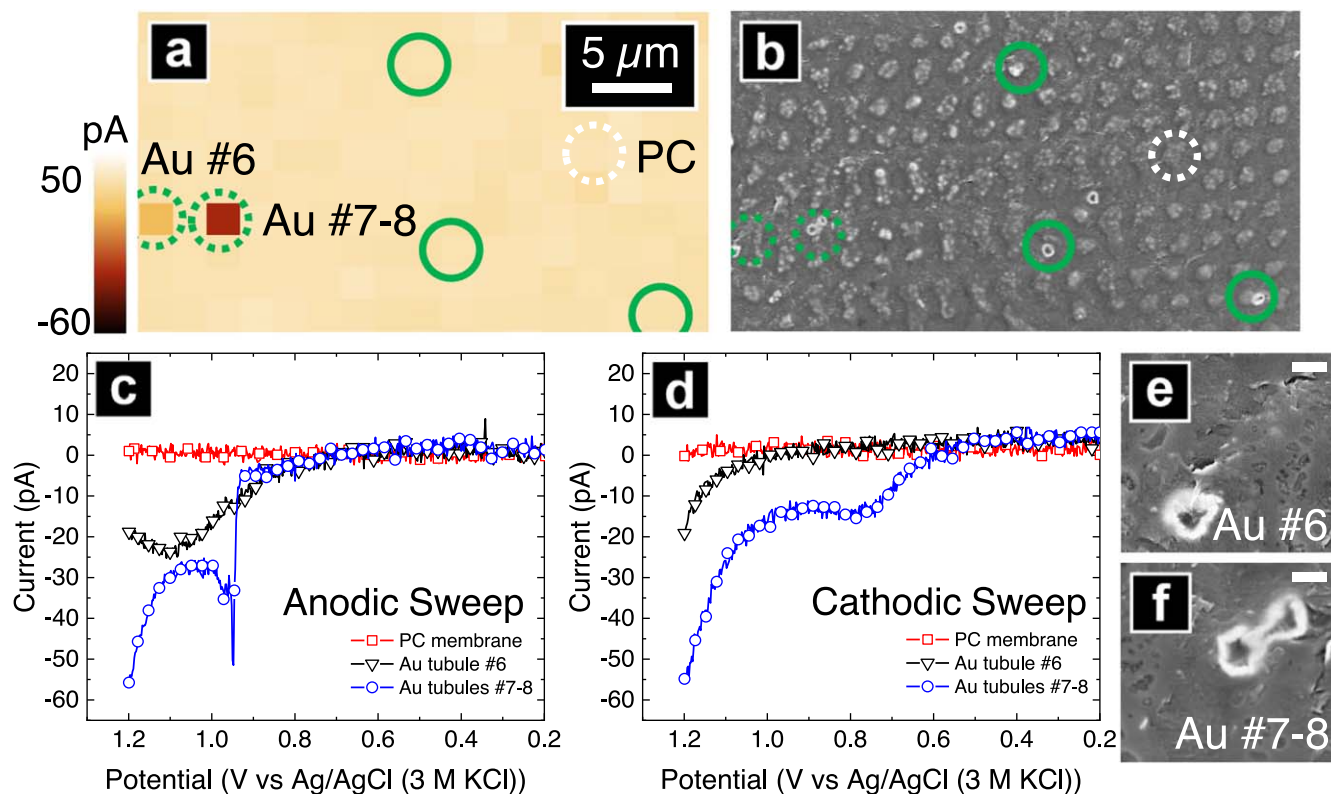
Figure 5. (a) SECCM cyclic voltammetric (CV) map for hydrazine electrooxidation on a nanoelectrode ensemble (NEE) at a substrate bias of 1.2 V vs Ag/AgCl (3 M KCl) and (b) correlative electron micrograph of the same area. The scale bar in Fig. 5a applies to Fig. 5b. (c) Anodic and (d) cathodic voltammetric sweeps at 3 positions: polycarbonate (PC) membrane, Au tubule #6, and Au tubules #7–8. (e)–(g) High-resolution electron micrographs of the Au tubules (Au tubule #6–8, respectively) exhibiting electrocatalytic current (scale bar = 500 nm). The solution in the pipette was aqueous 2 mM $N_2H_4 \cdot H_2O$ and 10 mM $HClO_4$ and the scan rate was 0.5 V s^{-1}. The spacing between droplet contact spots was 2 μm. The solid green circles denote positions where Au tubules were contacted by the SECCM droplet, but no enhanced current response was recorded.
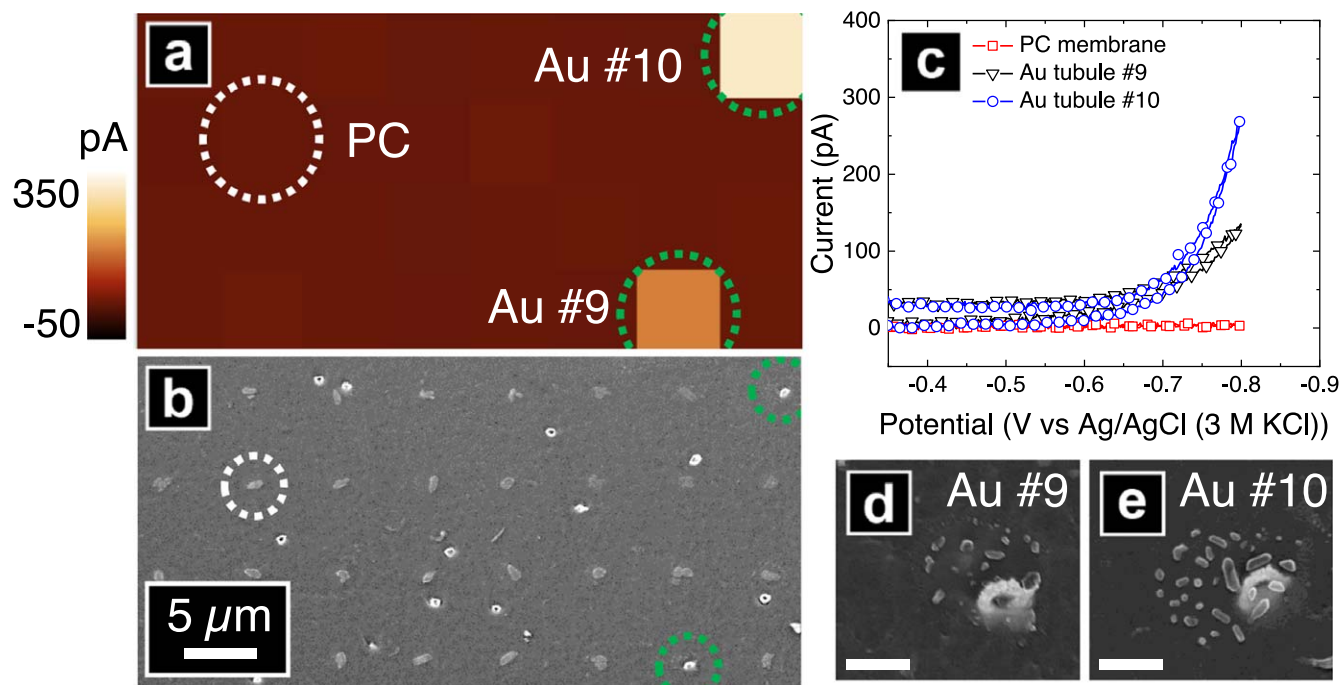

Figure 6. (a) SECCM cyclic voltammetric (CV) map for HER on a nanoelectrode ensemble (NEE) at a substrate bias of -0.8 V vs Ag/AgCl (3 M KCl) and (b) correlative electron micrograph of the same area. The scale bar in Fig. 6b applies to Fig. 6a. CVs at 3 positions: polycarbonate (PC) membrane and Au tubules #9 and #10. High-resolution electron micrographs of (d) Au tubule #9 and (e) Au tubule #10 (scale bar = 1 μm). The solution in the pipette was aqueous 10 mM $HClO_4$ and the scan rate was 0.5 V s^{-1}. The spacing between droplet contact spots was 6 μm.
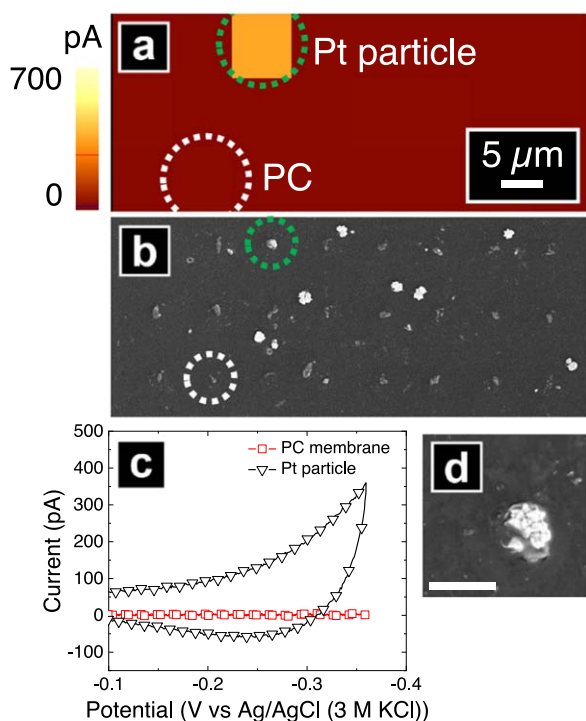
Figure 7. (a) SECCM cyclic voltammetric (CV) map of Pt particles deposited on a nanoelectrode ensemble (Pt-NEE) at a substrate bias of -0.35 V vs Ag/AgCl (3 M KCl) and (b) correlative electron micrograph of the same area. The scale bar in Fig. 7a applies to Fig. 7b. (c) CVs at 2 positions: polycarbonate (PC) membrane and a Pt particle. (d) High-resolution electron micrograph of a Pt particle (scale bar = 1 μm). The solution in the pipette was aqueous 10 mM $HClO_4$ and the scan rate was 0.5 V s^{-1}. The spacing between droplet contact spots was 6 μm.

$C = AC_d$, where C = capacitance in the measurement, A = surface area of the particle, and C_d = double layer capacitance.[41] In comparison, the double layer capacitance from macroscale measurements of NEEs, prepared by Au electroless deposition, can be 20–40 μC cm^{-2} for a NEE with 30 nm diameter electrodes, a geometric area of 0.079cm^2, a pore density of 6 x 10^8 pore cm^{-2}, and at scan rate 0.1 V s^{-1}.[2,41] The double layer capacitance estimated from SECCM measurements on the Pt particle is similar to macroscale measurements of NEEs, although this conclusion should be taken *cum grano salis*. The double layer capacitance estimation from SECCM does not account for the surface roughness of the Pt particle and capacitance from the SECCM measurement was inferred from one voltammogram instead of calculating the capacitance from a controlled potential measurement or from extracting C_d from a plot relating current in the non-faradaic region of the CV to the scan rate. The Pt particle, with a particle diameter of $\sim$900 nm, was fully encapsulated by the SECCM droplet as confirmed by SEM in Fig. 7d. Additional SECCM CVs and correlative electron micrographs on Pt-NEEs can be found in Fig. S5. Of note, the voltammetric response recorded at Pt particles, in Figs. 7 and S5, show a shifted CV response towards more positive potentials relative to SECCM measurements on the NEE in Fig. 6. This positive shift occurs because Pt, which has a near zero free energy of hydrogen adsorption indicative of near optimal hydrogen adsorption to the metal surface, is a superior catalyst for HER compared to Au, which has weaker hydrogen adsorption and thus poorer electrocatalytic activity.[42,43]

Conclusions

In summary, single-entity electrocatalytic measurements by SECCM were conducted on NEEs and Pt-NEEs which were prepared by Au electroless deposition on porous PC membrane

templates. NEEs are presented as a proof-of-concept sample type for electrochemical imaging in which the underlying substrate is an insulator, and the conductive tubules or particles are patterned on the surface according to the density of pores in the membrane template. Accordingly, the electrocatalytic response is solely attributed to the Au tubules or Pt particles because the support is non-conductive. Analysis of NEEs with SECCM underscores the advantage of SECCM mapping using a dual barrel probe configuration in which localized electrocatalytic measurements are carried out on both the insulating PC membrane and the conductive Au tubules in the NEE. Electrocatalytic reactions explored at NEEs in this report include HER, Au surface oxidation, and hydrazine oxidation. Here, standard electrocatalytic reactions were examined. We expect that the inert nature of the polymeric substrate provides a platform that may be useful for studies of electrocatalytic materials that are comparable to or less active than typical substrates like glassy carbon, which may be important in initial stages of catalyst development. Additionally, in the future, more elegant methods to prepare patterned electrode arrays[44–47] on insulating substrates that correlate the spacing between SECCM droplet landing spots with nanoelectrode position could be targeted which would allow higher density data sets to be recorded via a similar approach.

ORCID

Lane A. Baker https://orcid.org/0000-0001-5127-507X

References

1. C. R. Martin, M. Nishizawa, K. Jirage, and M. Kang, *J. Phys. Chem. B*, **105**, 1925 (2001).
2. V. P. Menon and C. R. Martin, *Anal. Chem.*, **67**, 1920 (1995).
3. M. Nishizawa, V. P. Menon, and C. R. Martin, *Science*, **268**, 700 (1995).
4. M. Lahav, E. A. Weiss, Q. Xu, and G. M. Whitesides, *Nano Lett.*, **6**, 2166 (2006).
5. C. G. Zoski, N. Yang, P. He, L. Berdondini, and M. Koudelka-Hep, *Anal. Chem.*, **79**, 1474 (2007).
6. F. Muench, E.-M. Felix, M. Rauber, S. Schaefer, M. Antoni, U. Kunz, H.-J. Kleebe, C. Trautmann, and W. Ensinger, *Electrochim. Acta*, **202**, 47 (2016).
7. J. Wang, M. Tian, T. E. Mallouk, and M. H. W. Chan, *J. Phys. Chem. B*, **108**, 841 (2004).
8. X. Li, E. Koukharenko, I. S. Nandhakumar, J. Tudor, S. P. Beeby, and N. M. White, *Phys. Chem. Chem. Phys.*, **11**, 3584 (2009).
9. M. E. T. Molares, V. Buschmann, D. Dobrev, R. Neumann, R. Scholz, I. U. Schuchert, and J. Vetter, *Adv. Mater.*, **13**, 62 (2001).
10. R. M. Penner and C. R. Martin, *Anal. Chem.*, **59**, 2625 (1987).
11. Y.-L. Tai and H. Teng, *Chem. Mater.*, **16**, 338 (2004).
12. Y. Kobayashi and C. R. Martin, *Anal. Chem.*, **71**, 3665 (1999).
13. B. Jirage Kshama, J. C. Hulteen, and C. R. Martin, *Science*, **278**, 655 (1997).
14. T. Ito, A. A. Audi, and G. P. Dible, *Anal. Chem.*, **78**, 7048 (2006).
15. A. K. Bentley, M. Farhoud, A. B. Ellis, A.-M. L. Nickel, G. C. Lisensky, and W. C. Crone, *J. Chem. Educ.*, **82**, 765 (2005).
16. H. Q. Cao, Y. Xu, J. M. Hong, H. B. Liu, G. Yin, B. L. Li, C. Y. Tie, and Z. Xu, *Adv. Mater.*, **13**, 1393 (2001).
17. J. Experton, X. Wu, G. Wang, and C. R. Martin, *ChemElectroChem*, **5**, 3113 (2018).
18. S. N. Bush, J. Experton, A. T. de La Serve, E. P. Johnson, and C. R. Martin, *J. Electrochem. Soc.*, **167**, 132501 (2020).
19. C.-H. Chen, L. Jacobse, K. McKelvey, S. C. S. Lai, M. T. M. Koper, and P. R. Unwin, *Anal. Chem.*, **87**, 5782 (2015).
20. A. G. Güell, A. S. Cuharuc, Y.-R. Kim, G. Zhang, S.-Y. Tan, N. Ebejer, and P. R. Unwin, *ACS Nano*, **9**, 3558 (2015).
21. M. Choi, N. P. Siepser, S. Jeong, Y. Wang, G. Jagdale, X. Ye, and L. A. Baker, *Nano Lett.*, **20**, 1233 (2020).
22. C. L. Bentley, M. Kang, F. M. Maddar, F. Li, M. Walker, J. Zhang, and P. R. Unwin, *Chem. Sci.*, **8**, 6583 (2017).

23. C. L. Bentley, C. Andronescu, M. Smialkowski, M. Kang, T. Tarnev, B. Marler, P. R. Unwin, U.-P. Apfel, and W. Schuhmann, *Angew. Chem. Int. Ed.*, **57**, 4093 (2018).
24. R. G. Mariano, M. Kang, O. J. Wahab, I. J. McPherson, J. A. Rabinowitz, P. R. Unwin, and M. W. Kanan, *Nat. Mater.*, **20**, 1000 (2021).
25. Y. Wang, E. Gordon, and H. Ren, *Anal. Chem.*, **92**, 2859 (2020).
26. B. Tao, L. C. Yule, E. Daviddi, C. L. Bentley, and P. R. Unwin, *Angew. Chem. Int. Ed.*, **58**, 4606 (2019).
27. C. L. Bentley, M. Kang, and P. R. Unwin, *J. Am. Chem. Soc.*, **139**, 16813 (2017).
28. A. G. Güell, K. E. Meadows, P. V. Dudin, N. Ebejer, J. V. Macpherson, and P. R. Unwin, *Nano Lett.*, **14**, 220 (2014).
29. B. Paulose Nadappuram, K. McKelvey, J. C. Byers, A. G. Güell, A. W. Colburn, R. A. Lazenby, and P. R. Unwin, *Anal. Chem.*, **87**, 3566 (2015).
30. S. L. Kinnear, K. McKelvey, M. E. Snowden, M. Peruffo, A. W. Colburn, and P. R. Unwin, *Langmuir*, **29**, 15565 (2013).
31. D. Battistel, G. Pecchielan, and S. Daniele, *ChemElectroChem*, **1**, 140 (2014).
32. S. E. Alden, N. P. Siepser, J. A. Patterson, G. S. Jagdale, M. Choi, and L. A. Baker, *ChemElectroChem*, **7**, 1084 (2020).
33. P. Saha, J. W. Hill, J. D. Walmsley, and C. M. Hill, *Anal. Chem.*, **90**, 12832 (2018).
34. S. C. S. Lai, P. V. Dudin, J. V. Macpherson, and P. R. Unwin, *J. Am. Chem. Soc.*, **133**, 10744 (2011).
35. G. Dietz Jr, R. M. Skomoroski, and R. G. Zobbi, "Method for Producing Alkali Metal Gold Sulfite." *U.S. Patent*, 3,966,880 (1976).
36. P. Scopece, L. A. Baker, P. Ugo, and C. R. Martin, *Nanotechnology*, **17**, 3951 (2006).
37. C. L. Bentley, R. Agoston, B. Tao, M. Walker, X. Xu, A. P. O'Mullane, and P. R. Unwin, *ACS Appl. Mater. Interfaces*, **12**, 44307 (2020).
38. T. Tarnev, H. B. Aiyappa, A. Botz, T. Erichsen, A. Ernst, C. Andronescu, and W. Schuhmann, *Angew. Chem. Int. Ed.*, **58**, 14265 (2019).
39. G. J. Brug, M. Sluyters-Rehbach, J. H. Sluyters, and A. Hemelin, *J. Electroanal. Chem.*, **181**, 245 (1984).
40. U. Oesch and J. Janata, *Electrochim. Acta*, **28**, 1237 (1983).
41. C. G. Zoski, *Handbook of Electrochemistry* (Elsevier, Amsterdam)892 (2007).
42. E. Skúlason, V. Tripkovic, M. E. Björketun, S. Gudmundsdóttir, G. Karlberg, J. Rossmeisl, T. Bligaard, H. Jónsson, and J. K. Nørskov, *J. Phys. Chem. C*, **114**, 18182 (2010).
43. Z. W. Seh, J. Kibsgaard, C. F. Dickens, I. Chorkendorff, J. K. Nørskov, and T. F. Jaramillo, *Science*, **355**, eaad4998 (2017).
44. C. Ma, N. M. Contento, L. R. Gibson, and P. W. Bohn, *ACS Nano*, **7**, 5483 (2013).
45. D. Han, L. P. Zaino, K. Fu, and P. W. Bohn, *J. Phys. Chem. C*, **120**, 20634 (2016).
46. M. E. Sandison and J. M. Cooper, *Lab Chip*, **6**, 1020 (2006).
47. M. Atighilorestani and A. G. Brolo, *Anal. Chem.*, **89**, 9870 (2017).